ACS OMEGA

Open Access

http://pubs.acs.org/journal/acsodf

Article

Effect of Polystyrene Microplastics on Pb(II) Adsorption onto a Loessial Soil (Sierozem) and Its Mechanism

Yin Zhang, Baowei Zhao,* Xin Zhang, Yingquan Li, Hui Liu, Jian Zhang, and Tao Wang

Cite This: *ACS Omega* 2024, 9, 32021−32032

Read Online

ACCESS | Metrics & More | Article Recommendations

ABSTRACT: Microplastics (MPs) have received significant attention recently. However, their influence on soil heavy metal adsorption remains unclear. The effect of polystyrene (PS) MPs on the adsorption of Pb(II) onto a loessial soil (sierozem) was studied by batch experiments in single soil (S), soil with 1 mm PS (S-PS1), and soil with 100 μm PS (S-PS100) systems. The mechanisms of Pb(II) adsorption reduction were investigated. The adsorption of Pb(II) reached equilibrium within 12 h, and the pseudo-second-order model fitted the adsorption processes best. The Langmuir adsorption model provided a better fit to the isotherms, compared to the Freundlich one. The presence of PS decreased the level of adsorption of Pb(II). Larger PS particle size, dose, and fulvic acid (FA) concentration inhibited Pb(II) adsorption onto the soil. The solution pH value showed a positive correlation with the adsorption amount. The adsorption amounts (q_e) of Pb(II) in binary metal systems (Cu−Pb and Cd−Pb) were lower than those in single Pb systems, indicating the competitive adsorption among the ions. The adsorption amount presented a trend of S > S-PS100 > S-PS1. The primary mechanism on which PS reduced the adsorption of Pb(II) was the "dilution effect" of MPs. Conclusively, the presence of MPs might elevate the availability of heavy metals by reducing the soil's adsorption capacity for them and then amplifying the risk of heavy metal contamination and migration.

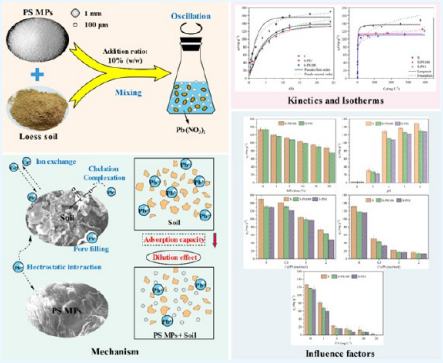

1. INTRODUCTION

Plastic products are extensively used in agriculture, construction, automobile manufacturing and product packaging, and other fields.[1] The discarded plastics in the environment are decomposed into microplastics (MPs, <5 mm) through the action of ultraviolet irradiation, hydrolysis, thermal oxidation, and biological activity.[2−4] Owing to their large specific surface area, strong hydrophobicity, and small particle size, MPs may carry many types of pollutants, including heavy metals and organic pollutants, in the water environment, to form composite pollution.[5,6] Numerous studies have documented that MPs alone, as well as those loading with other contaminants, can have detrimental effects on the health of aquatic organisms and vegetation.[7−9]

It is thought that the concentration of MPs in terrestrial soil ecosystems is 4−23 times more than that in the marine environment.[10] For example, in Harbin, Shandong, and Yunnan regions of China, the concentrations of MPs in agricultural soils were 198.32−1002.61,[11] 1.3−14.7,[12] and 7100−42,960 n·kg^{-1},[13] respectively. MPs were also discovered in the Loess Plateau with an abundance of 2982.34 n·kg^{-1}.[14] The MP levels in Swiss flood plain soils reached 593 n·kg^{-1},[15] and they were even as high as 67,500 mg·kg^{-1} in an industrial area in Sydney, Australia.[16] After entering the soil, MPs can significantly affect the soil physicochemical properties,[17,18] the growth and development of microorganisms, animals,[19,20] and crops.[21,22] The concern is that MPs can cause harm to soil ecosystems.[23−25] Therefore, the contamination of MPs in soil needs to receive adequate attention.

Meanwhile, heavy metals are also the main contaminants in soil. The China Soil Pollution Survey Bulletin (Ministry of Environmental Protection and Ministry of Land and Resources, 2014) reported that 19.4% of arable soil sites in China have heavy metal contamination exceeding safe levels. The main pollutants identified are Cu, As, Cd, Ni, Pb, and Hg. Soil MP pollution and heavy metal pollution areas are commonly overlapped, forming a composite pollution,[26] which in turn affects soil-associated microorganisms, animals, and plants.[27,28] Researchers[29] extracted different contents of Cu, Cd, and Pb from soil MP particles, proving that MPs in soil have adsorptive properties for heavy metals. The addition of high-density polythene (HDPE) reduced the soil's adsorption capacity for Cd and increased its desorption capacity. The inhibitory effect on the adsorption process was

Received: April 21, 2024
Revised: July 4, 2024
Accepted: July 5, 2024
Published: July 13, 2024

more pronounced with larger particle sizes and higher addition amounts.[30] MPs can impact the adsorption of heavy metals in soil observably, altering their distribution and form of heavy metals, which subsequently influences their bioavailability.[31] The possible impacts of MPs on heavy metals in soil are strongly influenced by various factors, including the properties of MPs (e.g., size, dose, type, and shape) and soil physicochemical indices (e.g., soil pH value and organic matter).[32,33] Polythene (PE) films were able to adsorb Cu and Ni in the soil, improving their bioavailability and toxicity.[34] Polystyrene (PS) fragments can increase the bioavailability of Cd,[35] while microbeads can reduce the bioavailability of Cd.[36] However, it has also been demonstrated that the presence of PE can alter the morphology of Cu, Cd, and Ni in soil from exchangeable speciation, carbonate-bounded forms, and Fe−Mn oxide-bound fraction to organic matter fractions, thus reducing the bioavailability.[37] These findings suggest the potential risk that MPs pose to soil ecosystems. Although the effects of MPs on soil adsorption of heavy metals have been studied, research on the mechanism of the effects of MPs is still limited, especially the laws and mechanisms of the environmental factor effect on the adsorption process are not clear. Therefore, it is necessary to study further the effects of MPs on soil-adsorbed heavy metals under different environmental conditions in order to further clarify the ecological risks of MPs.

Thus, in this paper, PS and Pb(II) were taken as the representative of MPs and heavy metals, respectively. The batch equilibrium experiments were conducted using single soil (S), soil with 1 mm PS (S-PS1), and soil with 100 μm PS (S-PS100) as the adsorbents. The adsorption dynamics and thermodynamics of Pb(II) in the PS-soil system were investigated. The effects of different particle sizes and doses of MPs, solution pH value, coexisting ions (Cu(II) and Cd(II)), and fulvic acid (FA) content on the adsorption of Pb(II) onto soil were discussed. At last, the effect mechanism of MPs on Pb(II) adsorption in soil was analyzed. The results could provide a theoretical foundation for understanding the impacts of MPs on heavy metal ecological risk in soil.

2. MATERIALS AND METHODS

2.1. Materials and Chemicals. PS were purchased from Zhongxin Plastics Co., Ltd., Dongguan, Guangdong, China, with particle sizes of 1 mm and 100 μm and densities of 1.04−1.06 g·cm^{-3}. To eliminate the influence of impurities on the PS surface, the PS were first ultrasonically cleaned twice using 5% dilute nitric acid and then repeatedly cleaned with deionized water. After being air-dried, these PS were stored in brown glass bottles. $Pb(NO_3)_2$, $Cd(NO_3)_2$, and NaOH were bought from Damao Chemical Reagent Factory, Tianjin, China. $CuCl_2$ was obtained from Kaixin Chemical Co., Ltd., Tianjin, China. Nitric acid was produced by the Guangfu Fine Chemical Research Institute, Tianjin, China. Every chemical agent in the experiment was analytically pure. Fulvic acid was produced by Shanghai Yuanye Biotechnology Co., Ltd., with a molecular weight of 308.24 and a purity of 90%. The experimental water was deionized water.

The soil was collected from Anning District, Lanzhou, Gansu Province, China (36°11′N, 103°73′E). The soil type was sierozem with a medium loam texture. The impurities, such as stones and twigs, in the samples were picked out. The soil's physical and chemical characteristics were determined after air drying and screening via a 2 mm mesh sieve. The pH value of soil was assessed using a pH meter (PB-10, Shanghai Tec-Front Electronics Co., Ltd., China). Electrical conductivity (EC) was tested by using a conductivity meter (DDS-11A, Hangzhou Aolilong Instrument Co., China). The cation exchange capacity (CEC) was estimated by reference to national environmental protection standards (HJ889-2017). Organic matter content was quantified by the dilution heat method using a potassium dichromate. The concentration of Pb(II) was detected by using flame atomic absorption spectrophotometry (AA7000, SHIMADZU, Japan). After measurement, the pH value, EC, CEC, organic matter, and total Pb(II) of the original soil were 7.89, 1.47 (ms·cm^{-1}), 4.49 (cmol·kg^{-1}), 0.42 (%), and 0.38 (mg·kg^{-1}), respectively. For the soil and PS mixture, PS (1 mm, 100 μm) was uniformly mixed into the soil, with 10% (w/w) PS fraction, labeled as S-PS1 and S-PS100. A control group with a single soil without PS (labeled as S) was set up. When considering the effect of MP dose, the concentration of PS was set to 1, 5, 10, 15, and 20% (w/w).

2.2. Characterization of PS and Soil. In order to accurately investigate the changes in PS characteristics before and after adsorption, the experiment was set up with a treatment group of pure PS (1 mm and 100 μm). Soil and PS after adsorption experiments were separated, filtered, and dried for characterization tests together with the original samples. The surface images of PS were surveyed by a scanning electron microscope (SEM, Hitachi S4800, Japan). The specific surface area and pore size distribution of PS were measured by N_2 adsorption−desorption via the surface area and porosity analyzer (nova2000e, Quantachrome) based on the Brunauer−Emmett−Teller (BET) equation. PS functional group alterations were investigated using Fourier transform infrared (FTIR, NEXUS 670) spectroscopy both before and after adsorption. The elemental composition shifts of the surface of PS samples were measured by X-ray photoelectron spectroscopy (XPS, Thermo Scientific ESCALAB 250Xi). The crystalline structures of PS were ascertained using an X-ray diffractometer (XRD, Smartlab, Japan). SEM, BET, XRD, FTIR, and XPS of the soil were obtained using the same methods as for PS.

2.3. Kinetics Experiment. 0.05 g portion of soil without or with 10% (w/w) PS and 50 mL of Pb(II) solution with a concentration of 250 mg·L^{-1} were added to flasks. The studies were conducted under a constant temperature condition of 25 ± 1 °C using a thermostatic oscillator operating at 270 rpm. The samples were taken at 0.25, 0.5, 1, 2, 4, 6, 8, 10, 12, 18, and 24 h, respectively. After centrifugation for 5 min, the supernatants were filtrated via a 0.22 μm filter membrane, and the Pb(II) concentrations were analyzed. For each assay, three replicates and two blank treatments without absorbent were contained.

The Pb(II) adsorption amount (q_t) (eq 1) was determined by calculating the difference between the total amount of Pb(II) added to the solution and the amount of Pb(II) retained. The equation is as follows

$$q_t = (C_0 - C_t)V/m \quad (1)$$

where q_t (mg·g^{-1}) refers to the adsorption quantity; t (h) indicates the contact time; C_0 (mg·L^{-1}) denotes the initial concentration of the Pb(II) solution; C_t (mg·L^{-1}) is the Pb(II) concentration at the reaction time; V (L) is the solution volume added; and m (g) is the mass of the absorbent.

https://doi.org/10.1021/acsomega.4c03809
ACS Omega 2024, 9, 32021−32032

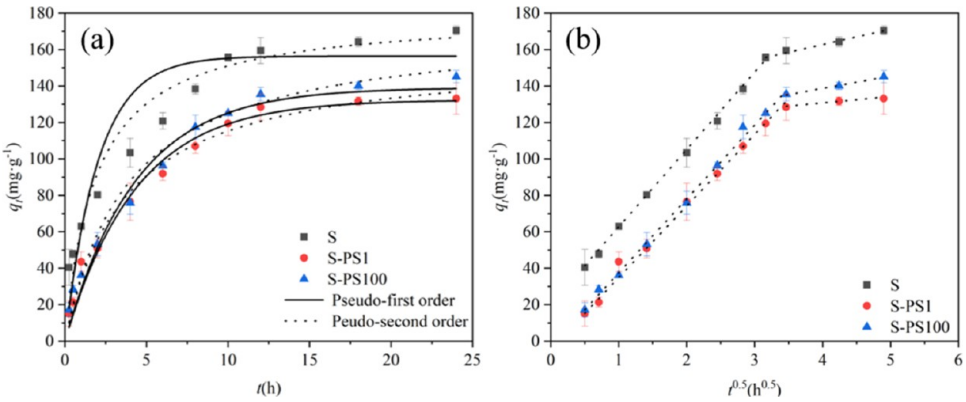

Figure 1. Plots of adsorptive amount of Pb(II) (q_t) versus reaction time (t) and kinetic fitting curve (a); plots of adsorptive amount of Pb(II) (q_t) versus $t^{0.5}$ and fitting curves using intraparticle diffusion model (b).

Table 1. Kinetic Parameters of Pb(II) Adsorption Fitted from the Pseudo-First-Order, Pseudo-Second-Order, and Intraparticle Diffusion Model

	pseudo-first-order model			pseudo-second-order model		
adsorbent	q_e (mg·g^{-1})	k_1 (h^{-1})	R^2	q_e (mg·g^{-1})	k_2 (mg·g^{-1}·h^{-1})	R^2
S	156.39	0.4901	0.9504	179.84	0.0029	0.9813
S-PS1	132.38	0.2303	0.9826	157.88	0.0017	0.9923
S-PS100	139.08	0.2305	0.9845	173.08	0.0014	0.9917
	intraparticle diffusion model					
adsorbent	B_1	$k_{p,1}$ (g·mg^{-1}·min$^{-0.5}$)	R^2	B_2	$k_{p,2}$ (g·mg^{-1}·min$^{-0.5}$)	R^2
S	20.26	42.45	0. 9989	128.87	8.45	0.9968
S-PS1	−4.4	39.26	0.9946	116.74	3.5	0.9399
S-PS100	−3.06	40.53	0.9994	111.65	6.76	0.9865

The pseudo-first-order model (eq 2), pseudo-second-order model (eq 3), and intraparticle diffusion model (eq 4) were applied to fit the adsorption kinetics

$$q_t = q_e(1 - e^{-k_1 t}) \quad (2)$$

$$q_t = k_2 q_e^2 t/(1 + k_2 q_e t) \quad (3)$$

$$q_t = k_i t^{0.5} + B \quad (4)$$

where k_1 (min^{-1}) and k_2 (g·mg^{-1}·min^{-1}) denote the pseudo-first-order and pseudo-second-order equilibrium rate constants, respectively. k_i (mg·g^{-1}·min$^{-0.5}$) indicates the model constant of intraparticle diffusion; q_t (mg·g^{-1}) is the adsorption amount at time t; q_e (mg·g^{-1}) refers to the equilibrium adsorption amount; and B (mg·g^{-1}) is a constant associated with the boundary layer.

2.4. Isothermal Adsorption. 0.05 g amount of adsorbents was put into 50 mL solution of various Pb(II) initial concentrations (5, 25, 50, 100, 150, 200, 250, 300, 400, and 500 mg·L^{-1}) at 25 °C. The equilibration time was set to 12 h based on kinetic experiments. The other reaction conditions were identical to those in the kinetic experiments. The supernatants were filtrated via a 0.22 μm filter membrane, and the equilibrium Pb(II) concentrations (C_e) were determined.

The Langmuir (eq 5) and Freundlich (eq 6) models were habituated to represent the adsorption isotherm of Pb(II) on three adsorbents (S, S-PS1, and S-PS100)

$$q_e = q_m K_L C_e/(1 + K_L C_e) \quad (5)$$

$$q_e = K_F C_e^n \quad (6)$$

where q_m (mg·g^{-1}) indicates the maximum adsorption capacity; K_L (L·mg^{-1}) is the Langmuir adsorption constant and K_F (L·g^{-1}) is the Freundlich partition coefficient indicating the strength of adsorption; n denotes the Freundlich intensity parameter and C_e (mg·L^{-1}) refers to the equilibrium concentration.

2.5. Effects of PS Dose, Solution pH, Coexisting Ions, and Fulvic Acid. To investigate the effect of varying PS doses, 1, 5, 10, 15, and 20% PS (w/w) concentration gradients were designed. The pH of the Pb(II) solution was manipulated to values of 2, 3, 4, 5, and 6 by adding 1 M NaOH and 1 M HNO_3 to examine the impact of pH. The concentrations of fulvic acid 1, 3, 5, 10, and 20 mg·L^{-1} were selected to explore its effect on Pb(II) adsorption. The Pb−Cd and Pb−Cu binary systems were constructed by using $Cd(NO_3)_2$ and $CuCl_2$, respectively. In order to research the impact of coexisting ions on the adsorption of Pb(II), the ionic molar ratios of Cd/Pb (or Cu/Pb) were maintained as 0.5:1, 1:1, and 2:1. The sampling and analysis methods were the same as thermodynamic experiments.

2.6. Analytical Method. The concentrations of Pb(II) in all experimental samples were determined by flame atomic absorption spectrometry (AA7000, SHIMADZU, Japan). The acetylene flow rate, lamp current, measured wavelength, and slit width were 1.5 L·min^{-1}, 2 mA, 283.3 nm, and 0.7 nm, respectively.

3. RESULTS AND DISCUSSION

3.1. Adsorption Kinetics. The adsorptive amount (q_t) of S, S-PS100, and S-PS1 for Pb(II) versus reaction time (t) is illustrated in Figure 1a. At the initial stage, the adsorption rate

https://doi.org/10.1021/acsomega.4c03809
ACS Omega 2024, 9, 32021−32032

of Pb(II) on the three adsorbents was very rapid. After 8 h, the adsorption rate increased slowly, and adsorption eventually reached equilibrium at 12 h. The phenomenon was attributed to more adsorptive sites on adsorbents being utilized, and the Pb(II) concentration was high and had a strong mass transfer drive at the initial stage. The quantity of adsorption sites gradually decreased and eventually reached saturation with time. As a result, the adsorption amount increased slowly and reached equilibrium.[38]

The adsorption behaviors of Pb(II) on three adsorbents were analyzed via fitting the adsorption data using kinetic models, and the findings are listed in Table 1 and Figure 1a. The R^2 value obtained from the pseudo-second-order model was between 0.9813 and 0.9917, surpassing those from the pseudo-first-order model (0.9504−0.9845). The fitted adsorption capacity (q_e) derived from the pseudo-second-order model was in good agreement with the testing data (Figure 1a). The pseudo-first-order model is generally based on the hypothesis that adsorption is controlled by a diffusion step. The pseudo-second-order model assumes that the chemisorption involving electron transfer, electron sharing, complexation between the adsorbent, and the adsorbate is the principal cause for controlling the adsorption process.[39] This indicates that the chemical sorption process might be the rate-limiting step in the adsorption of Pb(II) from soil or mixtures of PS and soil.

As shown in Table 1, the rate constants k_2 are shown in the order of S > S-PS1 > S-PS100, where a maximum reduction of 0.0015 mg·g^{-1}·h^{-1} was noticed. While the order of q_e was S > S-PS100 > S-PS1, the two particle sizes of PS caused a decrease in q_e by 21.96 mg·L^{-1} (1 mm) and 6.76 mg·L^{-1} (100 μm), respectively. This observation suggests that PS significantly reduced the adsorption ability of soil for Pb(II). Zhang et al.[30] discovered that the inclusion of 1% HDPE in soil reduced Cd adsorption, which is consistent with the results of our study. Many previous studies have demonstrated that MPs with smaller particle sizes generally exhibit a greater ability to adsorb heavy metals.[40,41] In this experiment, the adsorption ability of Pb(II) on S-PS1 was lower than that on S-PS100, confirming that MPs of particle sizes exert distinct effects on the soil adsorption capacity.

The adsorption data were fitted via the intraparticle diffusion model to explore the speed control steps and the adsorption mechanism. Figure 1b and Table 1 present the fitting curves and parameters. The absorption process of Pb(II) on three adsorbents included two stages. The initial phase was the diffusion of Pb(II) to the soil and PS surface through the liquid film (liquid film diffusion stage), while the second phase was the slow adsorption (intraparticle diffusion stage).[42] As illustrated in Table 1, the diffusion rate constant $k_{p,1} > k_{p,2}$ and the boundary layer $B_1 < B_2$. These observations further indicate that the diffusion process of Pb(II) onto adsorbents is initially rapid mainly because of the abundance of adsorption sites in the early phases of adsorption. However, as the adsorption approaches saturation in the first phases, the absorption sites on the inner surfaces of the adsorbent become occupied, resulting in an increased resistance to Pb(II) diffusion. Additionally, the boundary layers B_1 and B_2 were not 0, and the fitting lines did not cross the origin point. This suggests that particle internal diffusion is not the only rate-controlling step of Pb(II) adsorption on adsorbents. Instead, the adsorption rate may be jointly commanded by surface adsorption and intraparticle diffusion. The diffusion rate constants ($k_{p,1}$, $k_{p,2}$) of the three adsorbents show a pattern of S > S-PS100 > S-PS1, verifying that the adsorption rate was reduced by the addition of MPs, being consistent with the findings of the pseudo-second-order kinetic.

3.2. Adsorption Isotherm. Figure 2 reflects the variation of the adsorption amount (q_e) with the equilibrium concentration (C_e) of Pb(II) in solution. When the Pb(II) equilibrium concentration was less than 50 mg·L^{-1}, the adsorption amounts by the three adsorbents were positively correlated to the equilibrium concentration. As the equilibrium concentration increased, the adsorption amount gradually tended to be balanced. This might be ascribed to the fact that when the concentration of Pb(II) in solution grew, the adsorption sites on soil and PS surfaces steadily decreased and adsorption approached saturation.

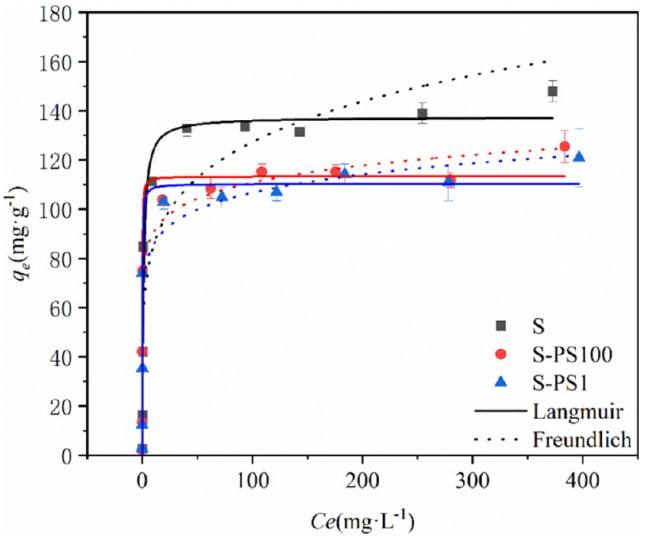

Figure 2. Plots of the equilibrium adsorptive amount of Pb(II) (q_e) versus the equilibrium concentration of Pb(II) (C_e) and Langmuir and Freundlich isotherm fitting for the adsorption of Pb(II).

The Langmuir isotherm assumes a uniform adsorbent surface, no interaction between adsorbent molecules, a dynamic equilibrium for adsorption, and monolayer adsorption. The Freundlich equation can be used to represent both monolayer adsorption and multilayer adsorption on heterogeneous surfaces.[43] Figure 2 and Table 2 display the fitting curves and parameters for the Langmuir and Freundlich equations. The Langmuir model (R^2 = 0.9491−0.9796) fitted the results better compared to the Freundlich model (R^2 = 0.8110−0.9633). Such findings indicate that Pb(II) adsorption on soil and soil−PS mixtures incorporates both physical and chemical adsorption mechanisms. The maximum adsorption, as inferred from the Langmuir model, showed the same tendency as that of the experimental data. The q_m values by three adsorbents showed the order of S > S-PS100 > S-PS1, and soils with two particle sizes of PS added showed a decrease of 24.10 mg·g^{-1} (100 μm) and 27.10 mg·g^{-1} (1 mm), respectively, compared to soils without PS. The reduction was more pronounced as the particle size of PS increases. Other researchers[44,45] have also found that the addition of PE reduced the adsorption of Zn and Cd onto the soil and that the smaller the PE particle size, the less pronounced the effect on the adsorption, which is in line with the result of the present study. Based on the previous experiments, the maximum adsorption of Pb(II) was 0.020 mg·g^{-1} by PS100 and 0.011 mg·g^{-1} by PS1, which were

https://doi.org/10.1021/acsomega.4c03809
ACS Omega 2024, 9, 32021−32032

Table 2. Fitting Parameter Values Using Langmuir and Freundlich Isotherm Parameter Values

	Langmuir			Freundlich		
absorbent	q_m (mg·g^{-1})	K_L (L·mg^{-1})	R^2	K_F	n	R^2
S	137.4610	0.9020	0.9491	56.7083	5.6938	0.8110
S-PS100	113.3490	9.6379	0.9752	73.9774	11.3878	0.9633
S-PS1	110.3575	5.9354	0.9796	68.5105	10.3831	0.9553

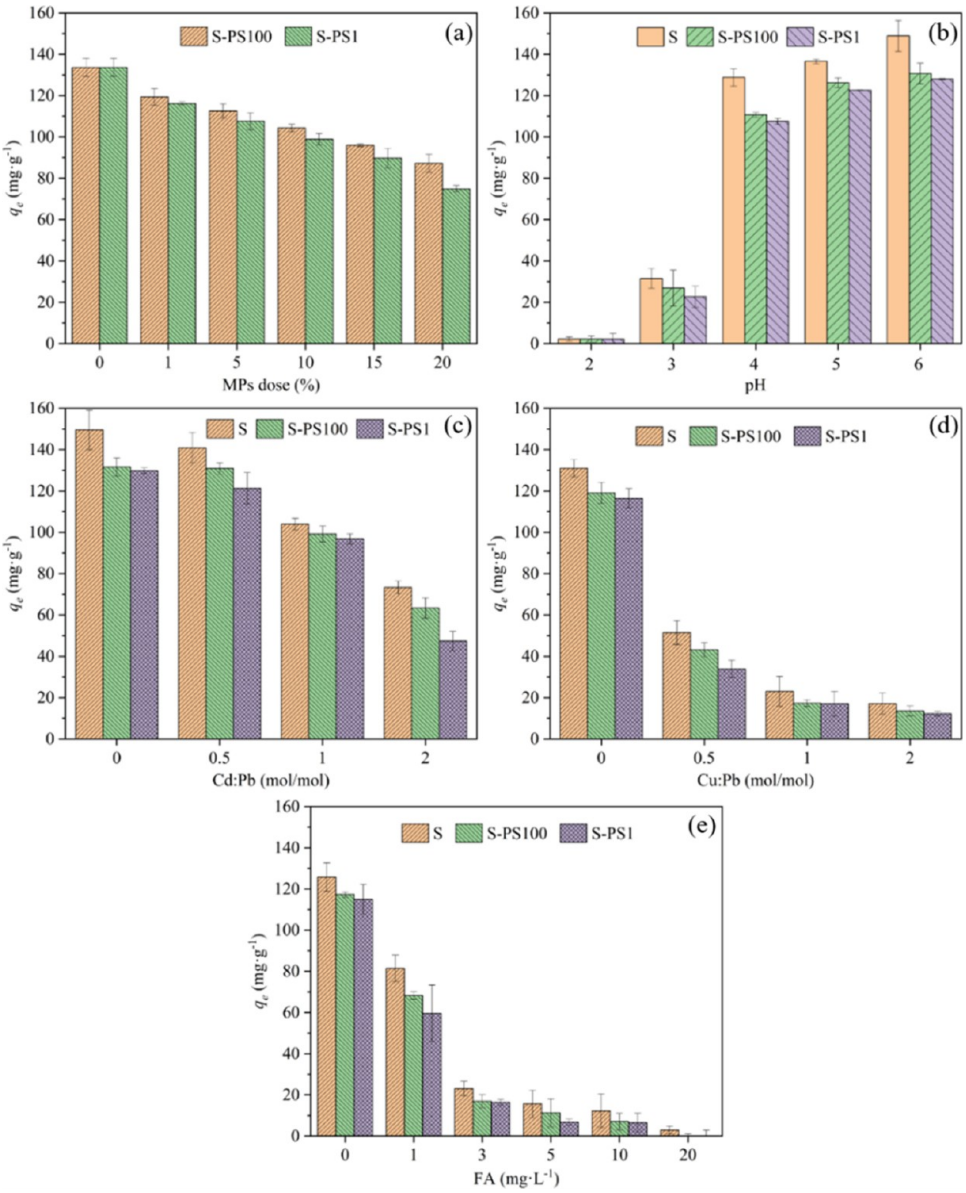

Figure 3. Effect of PS dose (a), pH (b), coexisting ions Cd (c) and Cu (d), and FA concentration (e) on Pb(II) adsorption.

significantly lower than that of the pure soil used in this study (137.46 mg·g^{-1}), with similar conclusions drawn from others' researches.[40,41] This could explain why the soil with PS had a lower q_m than the pure soil.

3.3. Effects of Influencing Factors. Figure 3a reflects the impact of the PS dose on the adsorption of Pb(II) on soil. With an increase in the proportion of PS, there was a clear decline in adsorption capacity. This effect was particularly noticeable with PS particles that have a size of 1 mm. Increasing the PS dose from 0 to 20% resulted in a decrease in q_e from 133.63 to 74.81 mg·g^{-1}. The content of PS was negatively correlated to the adsorption ability of Pb(II) in soil. The observed phenomenon might be attributed to the soil dilution effect resulting from the addition of MPs to the soil.[30] As the dose of PS increases, the proportion of PS per unit mass of soil also increases. This brings about a decrease of the adsorption site amounts in the soil. As mentioned above, the adsorption ability of PS for Pb(II) was largely lower than that of the soil, resulting in the decline of the soil−PS mixture adsorption capacity.

The pH value significantly affects the absorption behavior of heavy metals on soils via modifying the adsorbent surface charge.[46] Pb(II) was easy to hydrolyze and form precipitate under alkaline condition.[47] Therefore, the pH of ≤6 conditions

https://doi.org/10.1021/acsomega.4c03809
ACS Omega 2024, 9, 32021−32032

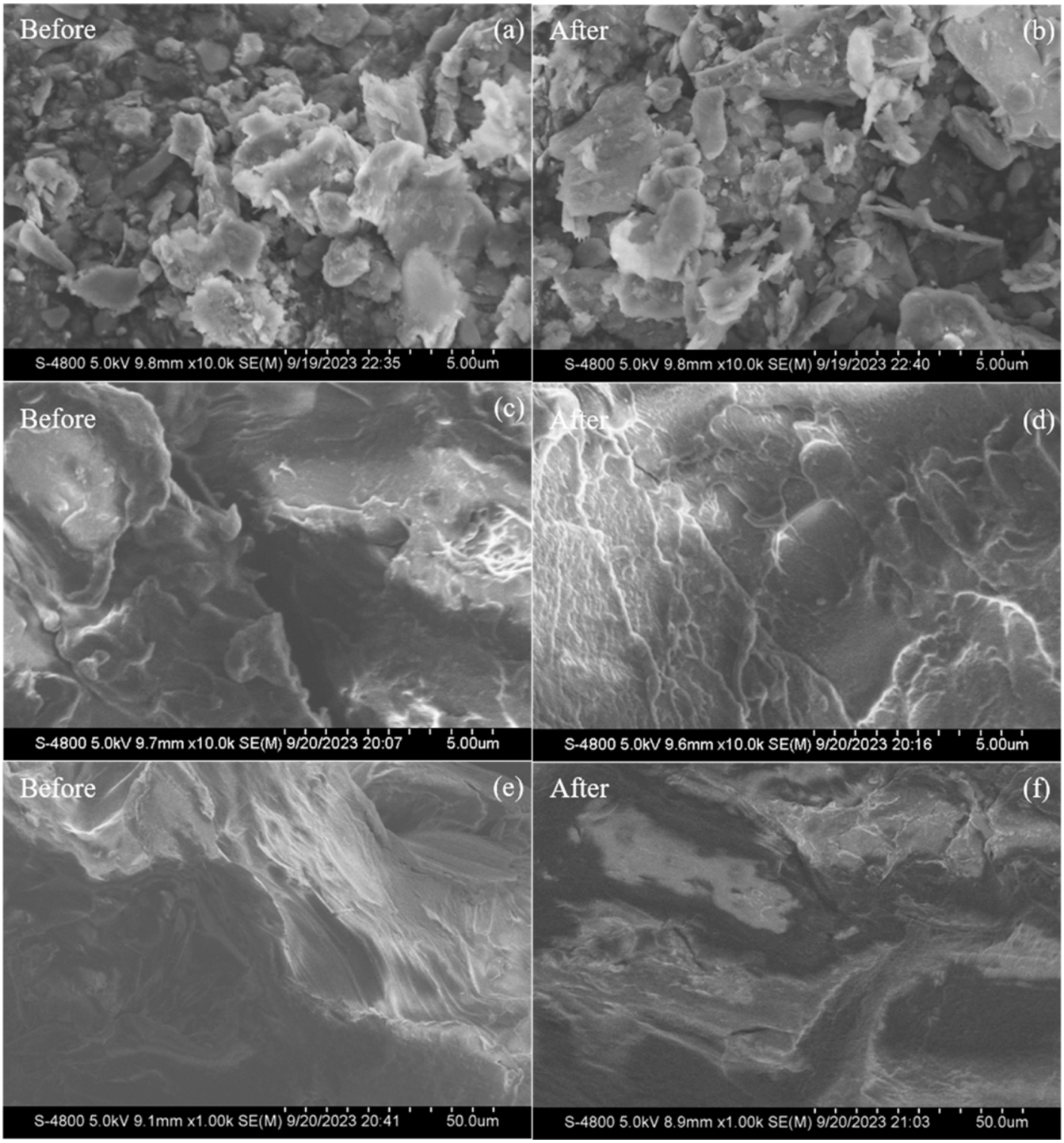

Figure 4. SEM images of soil and PS before and after adsorption. Soil (a, b), PS: 100 μm (c, d), and 1 mm (e, f).

was selected in this experiment to avoid the precipitation of metal oxides affecting the results. Figure 3b delineates the impact of different pH levels on the adsorption of Pb(II) with the three adsorbents. The findings revealed that an increase in the pH value led to a significant increase in the q_e of Pb(II). When the solution pH value increased from 2 to 6, the q_e of S, S-PS100, and S-PS1 increased from 2.19, 2.19, and 2.11 to 148.86, 130.63, and 127.93 mg·g^{-1}, respectively. The changes by S-PS100 and S-PS1 were not as drastic as those by pure soil. Under the same pH value, the extent of q_e showed the order of S > S- PS100 > S-PS1, reflecting that the PS reduced the adsorption of Pb(II) onto soil. Interestingly, the impact of PS on adsorption was not significant at pH = 2. This might be due to the competitive adsorption between H^+ and Pb(II) caused by the high concentration of H^+ in the solution at lower pH. According to available researches, the point of zero charge pH_{pzc} for PS is around 3.[47] This means that when pH < 3, the PS surface might be positively charged and mutually exclusive with Pb(II). This resulted in poor absorption of Pb(II) on the three adsorbents at lower pH values. As the pH increased, the influence of H^+ was weakened, and the negative charges on the surface of hydrated oxide, clay mineral, and organic matter in

https://doi.org/10.1021/acsomega.4c03809
ACS Omega 2024, 9, 32021−32032

soil were increased, which was conducive to soil adsorption. Around a pH of 5.5, Pb^{2+} tended to hydrolyze to form $Pb(OH)^{+}$, which could be deposited on the adsorbent, resulting in substantial adsorption.[48]

The impact of coexisting metal ions on the adsorption of Pb(II) by three adsorbents is shown in Figure 3c,d. When the Pb(II) concentration was constant, the q_e values of Pb(II) by three adsorbents in Cu−Pb and Cd−Pb systems were less than those in single Pb systems. The q_e decreased as the addition proportion of the coexisting ions increased. In the Cd−Pb system, the mole ratio goes from 0 to 2 ($mol \cdot mol^{-1}$), and the q_e by S, S-PS100, and S-PS1 decreased from 149.54, 131.59, and 129.79 to 73.32, 63.31, and 47.42 $mg \cdot g^{-1}$, respectively. Similarly, as for the Cu−Pb system, the q_e decreased from 131.00, 119.05, and 116.42 to 17.12, 13.56, and 12.21 $mg \cdot g^{-1}$. It has been demonstrated that in a multivariate system, both soil and PS exhibit adsorption properties for all metal ions.[49] The concurrent presence of Cu(II) (or Cd(II)) alongside Pb(II) initiated a competitive interaction on the adsorbent surface, thereby reducing the level of adsorption of Pb(II). In the binary systems, PS also reduced soil Pb(II) adsorption; the order of q_e was S > S-PS100 > S-PS1.

The Cu−Pb system exerted a more pronounced influence on the Pb(II) adsorption capacity than the Cd−Pb system. Some researchers have suggested that the selection coefficients of heavy metal ions in competitive adsorption systems are related to their physicochemical properties. The electronegativity of the three heavy metal ions followed the sequence Cu(II) > Pb(II) > Cd(II), while the hydrated ion radius was Pb(II) > Cu(II) > Cd(II).[50] On the basis of the distribution coefficient K_F of the Freundlich model, Jalali and Moradi[51] obtained that the selectivity coefficients of metal ions in calc soil were Cu(II) > Pb(II) > Cd(II). Compared to Cd(II), Pb(II) has a smaller ionic radius and a higher hydrolysis constant. Moreover, the hydroxyl compounds of Pb(II) are more readily adsorbed by the PS and soil, with a stronger competitive adsorption capacity, so the impact of Cd(II) on the adsorption of Pb(II) is not obvious.[52] Cu(II) possesses an electron layer structure with a non-noble gas configuration that readily forms hydrated ions in aqueous solution. Under identical conditions, Cu(II) has the highest selectivity coefficient, is more competitive, and therefore has a relatively greater influence on the adsorption of Pb(II).

Dissolved organic matter (DOM) is a mixture of compounds with different chemical properties, which is widely present in soil and water environments.[53] FA is a major component of DOM, and there is a complex interaction between DOM and the adsorption behavior of heavy metals. Figure 3e reveals that the adsorption of Pb(II) was significantly inhibited with an increasing FA concentration. As the FA concentration increased from 0 to 20 $mg \cdot L^{-1}$, the q_e by S, S-PS100, and S-PS1 decreased from 125.78, 117.31, and 114.97 to 2.90, 0.08, and 0.05 $mg \cdot g^{-1}$. The presence of numerous active functional groups in FA might be responsible for this phenomenon. These groups exhibit a strong binding affinity for heavy metals, leading to the formation of FA−metal complexes. The small molecular weight and high solubility of FA formed soluble complexes with heavy metals through complexation and chelation, thus inhibiting the precipitation and adsorption of heavy metals.[54,55] It was found that the influence of DOM on soil adsorption of heavy metals was different. On the one hand, DOM in organic materials can enhance the activity of heavy metals, thus inhibiting the adsorption of heavy metals by soil.[56,57] Another phenomenon was that DOM promotes the adsorption of heavy metals in soil, which fixes heavy metals in the soil to a certain extent.[58,59] This was closely related to the source of DOM, the type and concentration of heavy metals, and the physical and chemical properties of the soil.[54]

For soil−PS mixtures, the inhibition of the adsorption process by FA might also be related to the interaction between PS and FA. Research has shown that PS nanoplastics interact with soluble organics through the $\pi-\pi$ conjugation, causing the surface of PS particles to become rough instead of smooth.[60] It has been found that MPs can adsorb DOM through hydrophobic, intermolecular, and electrostatic effects.[61] The adsorption effect was more pronounced with smaller MP particle sizes. Consequently, a diminution of MP adsorption sites occurs, sequentially reducing the adsorptive quantity of Pb(II).

3.4. Adsorption Mechanism. SEM images of the soil and PS before and after adsorption are depicted in Figure 4a−f. There were many scattered particles and voids on the surface of soil particles, which could provide active sites for the absorption of Pb(II). After adsorption, the soil showed more complex surface characteristics and roughness, which might be attributed to the combination of Pb(II) and substances in the soil to form a precipitate.[62] Both sizes of PS showed irregular shapes and partial cracks, but the surface complexity was significantly lower than that of soil. The results revealed that the adsorption sites of PS were less than that of soil, and the 1 mm PS was particularly obvious. The specific surface area and pore size distribution of soil and PS were measured and are listed in Table 3. The data also indicated that the soil possesses a superior adsorption capacity under the same conditions.

Table 3. BET Surface Structure Characteristics of Soil and PS (100 μm and 1 mm)

adsorbent	S_{BET} ($m^2 \cdot g^{-1}$)	pore volume ($cm^3 \cdot g^{-1}$)	pore diameter (nm)
S	9.166	0.032	3.808
PS100	1.53	0.012	3.432
PS1	0.009	0.008	3.432

To assess the impact of crystallinity on the adsorption behavior of Pb(II), XRD patterns of soil and PS before and after absorption were performed, as presented in Figure 5a,b. XRD results revealed that there are no apparent changes in the XRD patterns of both soil and PS, suggesting that the crystallinity was similar before and after adsorption, and no new crystalline phase was formed.

The changes of functional groups on the soil and PS surfaces before and after adsorption as revealed by FTIR are displayed in Figure 5c,d. The peak of soil (Figure 5c) at 873 cm^{-1} was the C−H swing deformation, and the band at 1432 cm^{-1} might be a $-CH_3$ bending vibration. The peak positions after adsorption were shifted from 873 and 1432 to 838 and 1391 cm^{-1}, respectively. The intensity of the peak at 2500 cm^{-1} was weakened. This shows that soil adsorption of Pb(II) occurs in addition to chemical adsorption. This is in accordance with the results of the kinetic studies. The major absorption peaks for PS (Figure 5d) were 2923 and 2846 cm^{-1} (C−H stretching vibration), 1597 and 1938 cm^{-1} (monosubstituted aromatic rings), 1488 and 1446 cm^{-1} (C−C stretched in the aromatic ring), and 749 and 695 cm^{-1} (bending vibration of C−H in monosubstituted benzene). The FTIR spectra of PS did not exhibit any new peaks after the absorption of Pb(II). Guo et

https://doi.org/10.1021/acsomega.4c03809
ACS Omega 2024, 9, 32021−32032

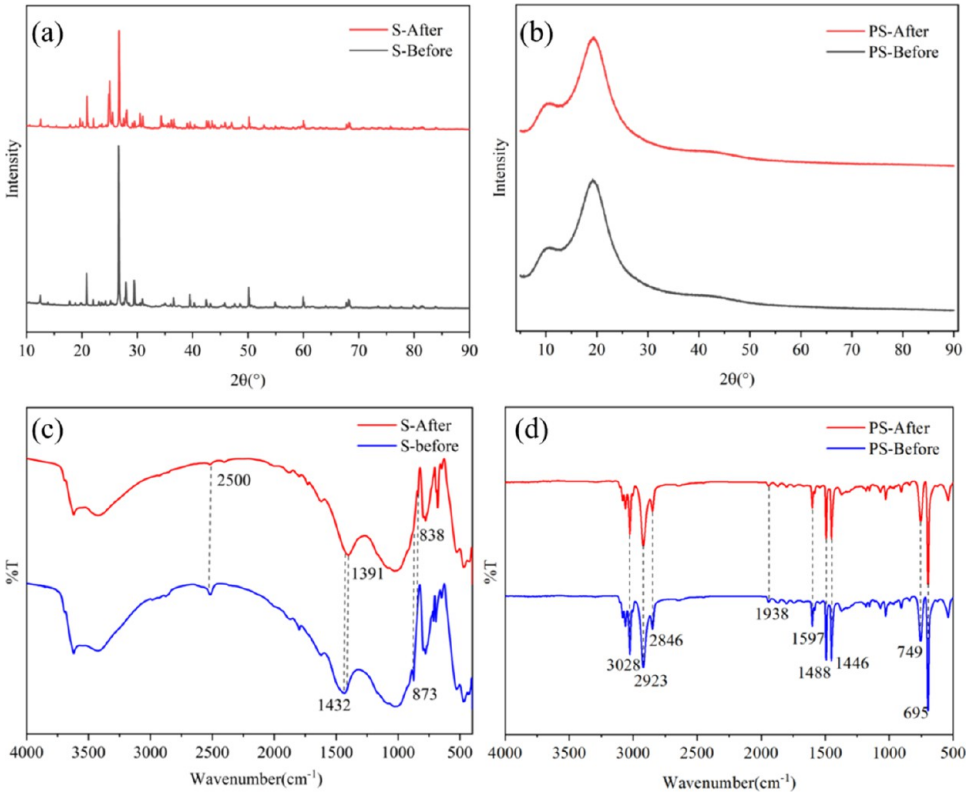

Figure 5. XRD (a, b) and FTIR (c, d) of soil and PS before and after adsorption.

al.[63] also found similar results for the characterization of four kinds of MPs (PP, PE, PVC, PS) after Cd adsorbed. This demonstrated that the adsorption of Pb(II) on PS was primarily a physical interaction.

The XPS characterization results of soil are presented in Figure 6a−d,g. Before adsorption, the C 1s (Figure 6a) in the soil was detected at 284.5 eV (CH_2−CH_2), 285.7 eV (C−OH, C−O), 289.1 eV (C═O, O═C−O), and 293.2 eV (C−CO_3). The spectra of O 1s (Figure 6c) were found at 530.5 eV (C═O, −OH), 531.1 eV (C═O), 531.9 eV (−OH, COOH), 532.5 eV (C═O, −OH), and 533.1 eV (C−OH, C−O−C, and O═C−O). After adsorption, XPS spectra of C 1s and O 1s were shifted somewhat (Figure 6b,d). For C 1s, the oxygen-containing functional group peak of 289.1 eV shifts significantly. This suggested that the oxygen-containing functional group played a role in this adsorption process. Regarding the O 1s, apart from the peak at 531.9 eV, the positions of the other peaks exhibit varying degrees. After adsorption, two peaks of Pb 4f at 138.6 and 143.5 eV can be attributed to Pb $4f_{7/2}$ and Pb $4f_{5/2}$, respectively, reflecting that Pb(II) has been adsorbed onto the soil (Figure 6g). Therefore, the functional groups C═O, C−OH, and ═C−O were essential for the adsorption process of Pb(II) in soil.

The results of the XPS characterization of PS are displayed in Figure 6e,f,h. Before adsorption (Figure 6e), the C 1s peaks of PS were located at 284.6, 285.1, and 288.9 eV, representing aromatic carbon, hydrocarbon, and aromatic oscillation, respectively.[64] After adsorption (Figure 6f), the aromatic oscillation peak moved to 291.4 eV, which means that there is a $\pi-\pi$ interaction. Two peaks of Pb 4f were detected at 139.1 and 144.02 eV after adsorption, confirming the adsorption of Pb(II) on the PS (Figure 6h). This means that the adsorption of Pb(II) on MPs was mainly physical sorption. In contrast to similar studies, Guo et al. attributed the adsorption mechanism of PS to the $\pi-\pi$ interaction.[65] In conclusion, physical interaction plays a crucial role in the process of adsorption of MPs. This outcome agrees with the FTIR results.

In summary, it is evident that while MPs exhibit an adsorptive effect on heavy metals, their adsorption capacity is markedly inferior compared to the soil; thereby, they will have a "dilution effect" after entering the soil. The binding ability between Pb(II) and microplastic particles weakens as the size of the particles increases, resulting in a more obvious dilution effect. The adsorption capacity of soil has a direct influence on the availability of Pb(II) in soil. As the previous research results confirmed, the addition of MPs will reduce the adsorption capacity of soil to Pb(II), thereby increasing the possibility of Pb(II) transport in the environment, which in turn poses a potential ecological risk.

4. CONCLUSIONS

Equilibrium for the adsorption of Pb(II) by all three adsorbents (S, S-PS100, S-PS1) was reached within 12 h. The adsorption process best conformed to the pseudo-second-order model ($R^2 > 0.9813$). The Langmuir model was found to be more appropriate for the adsorption process than the Freundlich one. Larger PS particle size, dose, and FA concentration inhibited the adsorption of Pb(II) from these soils. The pH of the solution was positively correlated with the adsorption capacity. In the presence of binary ions, the adsorption amount (q_e) and removal rate (R) of Pb(II) were lower in the binary systems (Cu−Pb and Cd−Pb) compared with the single Pb system caused by the competitive adsorption of the metal ions. The addition of PS resulted in a decrease in the adsorption amount (q_e) of Pb(II) on soil, with the order of S > S-PS100 > S-PS1. The impact of MPs on

https://doi.org/10.1021/acsomega.4c03809
ACS Omega 2024, 9, 32021−32032

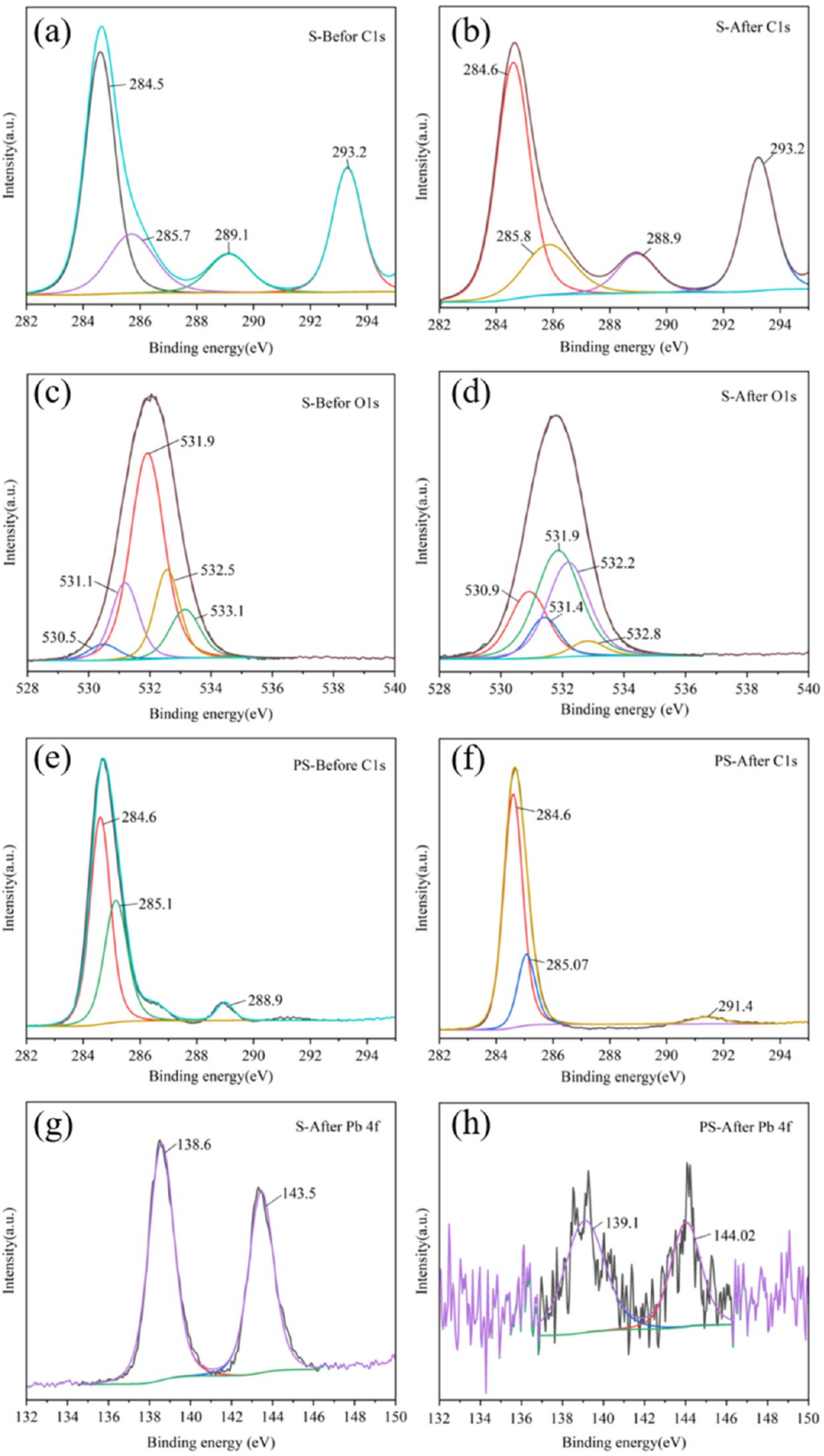

Figure 6. XPS spectra of the soil and PS before and after adsorption. C 1s for soil (a, b), O 1s for soil (c, d), C 1s for PS (e, f), Pb 4f for soil (g), and Pb 4f for PS (h).

https://doi.org/10.1021/acsomega.4c03809
ACS Omega 2024, 9, 32021−32032

the adsorption of heavy metals in soil is primarily determined by the "dilution effect".

AUTHOR INFORMATION

Corresponding Author

Baowei Zhao − *School of Environmental and Municipal Engineering, Lanzhou Jiaotong University, Lanzhou 730070 Gansu Province, P. R. China;* orcid.org/0000-0003-4224-6191; Email: baoweizhao@mail.lzjtu.cn

Authors

Yin Zhang − *School of Environmental and Municipal Engineering, Lanzhou Jiaotong University, Lanzhou 730070 Gansu Province, P. R. China*

Xin Zhang − *School of Environmental and Municipal Engineering, Lanzhou Jiaotong University, Lanzhou 730070 Gansu Province, P. R. China*

Yingquan Li − *School of Environmental and Municipal Engineering, Lanzhou Jiaotong University, Lanzhou 730070 Gansu Province, P. R. China*

Hui Liu − *School of Environmental and Municipal Engineering, Lanzhou Jiaotong University, Lanzhou 730070 Gansu Province, P. R. China*

Jian Zhang − *School of Environmental and Municipal Engineering, Lanzhou Jiaotong University, Lanzhou 730070 Gansu Province, P. R. China*

Tao Wang − *School of Environmental and Municipal Engineering, Lanzhou Jiaotong University, Lanzhou 730070 Gansu Province, P. R. China*

Complete contact information is available at: https://pubs.acs.org/10.1021/acsomega.4c03809

Author Contributions

Y.Z.: investigation, methodology, formal analysis, resources, and writing—original draft. B.Z.: conceptualization, formal analysis, resources, and writing—review and editing. X.Z.: visualization, methodology, and formal analysis. Y.L.: methodology, formal analysis, and resources. H.L.: methodology and formal analysis. J.Z.: methodology. T.W.: methodology.

Notes

The authors declare no competing financial interest.

ACKNOWLEDGMENTS

This study was supported by the National Natural Science Foundation of China (22166022, 22366025), the Natural Science Foundation of Gansu Province (23JRRA899), and the Gansu Provincial Department of Education: Excellent Graduate Student "Innovation Star" Project (2023CXZX-513).

REFERENCES

(1) Group, T. M. I. Plastics - the Facts 2017. An analysis of European plastics production, demand and waste data. *Tpe Magazine International: Thermoplastic Elastomers* **2018**, *9*, 93.

(2) Thompson, R. C.; Olsen, Y.; Mitchell, R. P.; Davis, A.; Rowland, S. J.; John, A. W. G.; McGonigle, D.; Russell, A. E. Lost at sea: Where is all the plastic, material and methods. *Science* **2004**, *304*, No. 838.

(3) Andrady, A. L. Microplastics in the marine environment. *Mar. Pollut. Bull.* **2011**, *62*, 1596−1605.

(4) Kwak, J. I.; An, Y. J. Microplastic digestion generates fragmented nanoplastics in soils and damages earthworm spermatogenesis and coelomocyte viability. *J. Hazard. Mater.* **2021**, *402*, No. 124034.

(5) Luo, Y.; Zhou, Q.; Zhang, H.; Pan, X.; Tu, C.; Li, L.; Yang, J. Pay attention to research on microplastic pollution in soil for prevention of ecological and food chain risks. *Bull. Chin. Acad. Sci.* **2018**, *33*, 1021−1030.

(6) Liu, G.; Zhu, Z.; Yang, Y.; Sun, Y.; Yu, F.; Ma, J. Sorption behavior and mechanism of hydrophilic organic chemicals to virgin and aged microplastics in freshwater and seawater. *Environ. Pollut.* **2019**, *246*, 26−33.

(7) Hermabessiere, L.; Paul-Pont, I.; Cassone, A.; Himber, C.; Receveur, J.; Jezequel, R.; El Rakwe, M.; Rinnert, E.; Rivière, G.; Lambert, C.; et al. Microplastic contamination and pollutant levels in mussels and cockles collected along the channel coasts. *Environ. Pollut.* **2019**, *250*, 807−819.

(8) Jiang, Y.; Yang, F.; Hassan Kazmi, S. S. U.; Zhao, Y.; Chen, M.; Wang, J. A review of microplastic pollution in seawater, sediments and organisms of the Chinese coastal and marginal seas. *Chemosphere* **2022**, *286*, No. 131677.

(9) Khoshmanesh, M.; Sanati, A. M.; Ramavandi, B. Co-occurrence of microplastics and organic/inorganic contaminants in organisms living in aquatic ecosystems: A review. *Mar. Pollut. Bull.* **2023**, *187*, No. 114563.

(10) Xu, B.; Huang, D.; Liu, F.; Alfaro, D.; Lu, Z.; Tang, C.; Gan, J.; Xu, J. Contrasting effects of microplastics on sorption of diazepam and phenanthrene in soil. *J. Hazard. Mater.* **2021**, *406*, No. 124312.

(11) Qing-xin, Y. U.; Shuo, L.; Li-na, M. A.; Zhi-yuan, M.; Tao-tao, L. I.; Lu-yao, C.; Meng, S. Analysis on the occurrence characteristics and influencing factors of microplastics in Harbin agricultural soils. *China Environ. Sci.* **2023**, *43*, 793−799.

(12) Zhou, Q.; Zhang, H.; Fu, C.; Zhou, Y.; Dai, Z.; Li, Y.; Tu, C.; Luo, Y. The distribution and morphology of microplastics in coastal soils adjacent to the Bohai Sea and the Yellow Sea. *Geoderma* **2018**, *322*, 201−208.

(13) Wang, T.; Zou, X.; Li, B.; Yao, Y.; Zang, Z.; Li, Y.; Yu, W.; Wang, W. Preliminary study of the source apportionment and diversity of microplastics: Taking floating microplastics in the South China Sea as an example. *Environ. Pollut.* **2019**, *245*, 965−974.

(14) Zhang, M.; Zheng, Y.; Li, J.; Liu, K.; Wang, H.; Gu, H.; Zhang, Z.; Guo, X. Distribution characteristics of microplastics in soil of Loess Plateau in northwest China and their relationship with land use type. *Sci. Total Environ.* **2023**, *868*, No. 161674.

(15) Scheurer, M.; Bigalke, M. Microplastics in Swiss Floodplain Soils. *Environ. Sci. Technol.* **2018**, *52*, 3591−3598.

(16) Fuller, S.; Gautam, A. A procedure for measuring microplastics using pressurized fluid extraction. *Environ. Sci. Technol.* **2016**, *50*, 5774−5780.

(17) Zhang, Y.; Cai, C.; Gu, Y.; Shi, Y.; Gao, X. Microplastics in plant-soil ecosystems: A meta-analysis. *Environ. Pollut.* **2022**, *308*, No. 119718.

(18) Zhou, J.; Xu, H.; Xiang, Y.; Wu, J. Effects of microplastics pollution on plant and soil phosphorus: A meta-analysis. *J. Hazard. Mater.* **2024**, *461*, No. 132705.

(19) Accinelli, C.; Abbas, H. K.; Bruno, V.; Nissen, L.; Vicari, A.; Bellaloui, N.; Little, N. S.; Thomas Shier, W. Persistence in soil of microplastic films from ultra-thin compostable plastic bags and implications on soil Aspergillus flavus population. *Waste Manage.* **2020**, *113*, 312−318.

(20) Zhang, X.; Li, Y.; Ouyang, D.; Lei, J.; Tan, Q.; Xie, L.; Li, Z.; Liu, T.; Xiao, Y.; Farooq, T. H.; et al. Systematical review of interactions between microplastics and microorganisms in the soil environment. *J. Hazard. Mater.* **2021**, *418*, No. 126288.

(21) Pignattelli, S.; Broccoli, A.; Renzi, M. Physiological responses of garden cress (L. sativum) to different types of microplastics. *Sci. Total Environ.* **2020**, *727*, No. 138609.

(22) Xu, G.; Liu, Y.; Yu, Y. Effects of polystyrene microplastics on uptake and toxicity of phenanthrene in soybean. *Sci. Total Environ.* **2021**, *783*, No. 147016.

(23) Rehman, M. Z. U.; Rizwan, M.; Ali, S.; Ok, Y. S.; Ishaque, W.; Saifullah; Nawaz, M. F.; Akmal, F.; Waqar, M. Remediation of heavy metal contaminated soils by using Solanum nigrum: A review. *Ecotoxicol. Environ. Saf.* **2017**, *143*, 236−248.

https://doi.org/10.1021/acsomega.4c03809
ACS Omega 2024, 9, 32021−32032

(24) Wong, J. K. H.; Lee, K. K.; Tang, K. H. D.; Yap, P. Microplastics in the freshwater and terrestrial environments: Prevalence, fates, impacts and sustainable solutions. *Sci. Total Environ.* **2020**, *719*, No. 137512.
(25) Deng, Y.; Wu, J.; Chen, J.; Kang, K. Overview of microplastic pollution and its influence on the health of organisms. *J. Environ. Sci. Health, Part A: Toxic/Hazard. Subst. Environ. Eng.* **2023**, *58*, 412−422.
(26) Duan, Q.; Li, J.; Liu, Y.; Chen, H.; Hu, H. Distribution of heavy metal pollution in surface soil samples in china: a graphical review. *Bull. Environ. Contam. Toxicol.* **2016**, *97*, 303−309.
(27) Chen, X.; Zheng, X.; Fu, W.; Liu, A.; Wang, W.; Wang, G.; Ji, J.; Guan, C. Microplastics reduced bioavailability and altered toxicity of phenanthrene to maize (Zea mays L.) through modulating rhizosphere microbial community and maize growth. *Chemosphere* **2023**, *345*, No. 140444.
(28) Li, Y.; Shi, X.; Qin, P.; Zeng, M.; Fu, M.; Chen, Y.; Qin, Z.; Wu, Y.; Liang, J.; Chen, S.; Yu, F. Effects of polyethylene microplastics and heavy metals on soil-plant microbial dynamics. *Environ. Pollut.* **2024**, *341*, No. 123000.
(29) Zhou, Y.; Liu, X.; Wang, J. Characterization of microplastics and the association of heavy metals with microplastics in suburban soil of central China. *Sci. Total Environ.* **2019**, *694*, 133791−133798.
(30) Zhang, S.; Han, B.; Sun, Y.; Wang, F. Microplastics influence the adsorption and desorption characteristics of Cd in an agricultural soil. *J. Hazard. Mater.* **2020**, *388*, No. 121775.
(31) An, Q.; Zhou, T.; Wen, C.; Yan, C. The effects of microplastics on heavy metals bioavailability in soils: a meta-analysis. *J. Hazard. Mater.* **2023**, *460*, No. 132369.
(32) Wang, F.; Wang, Q.; Adams, C. A.; Sun, Y.; Zhang, S. Effects of microplastics on soil properties: Current knowledge and future perspectives. *J. Hazard. Mater.* **2022**, *424*, No. 127531.
(33) Zhang, Q.; Guo, W.; Wang, B.; Feng, Y.; Han, L.; Zhang, C.; Xie, H.; Liu, X.; Feng, Y. Influences of microplastics types and size on soil properties and cadmium adsorption in paddy soil after one rice season. *Resour. Environ. Sustainability* **2023**, *11*, No. 100102.
(34) Li, M.; Liu, Y.; Xu, G.; Wang, Y.; Yu, Y. Impacts of polyethylene microplastics on bioavailability and toxicity of metals in soil. *Sci. Total Environ.* **2021**, *760*, No. 144037.
(35) Zhang, Z.; Li, Y.; Qiu, T.; Duan, C.; Chen, L.; Zhao, S.; Zhang, X.; Fang, L. Microplastics addition reduced the toxicity and uptake of cadmium to Brassica chinensis L. *Sci. Total Environ.* **2022**, *852*, No. 158353.
(36) Wang, F.; Zhang, X.; Zhang, S.; Zhang, S.; Adams, C. A.; Sun, Y. Effects of co-contamination of microplastics and Cd on plant growth and Cd accumulation. *Toxics* **2020**, *8*, No. 36.
(37) Yu, H.; Hou, J.; Dang, Q.; Cui, D.; Xi, B.; Tan, W. Decrease in bioavailability of soil heavy metals caused by the presence of microplastics varies across aggregate levels. *J. Hazard. Mater.* **2020**, *395*, No. 122690.
(38) Ma, F.; Zhao, H.; Zheng, X.; Zhao, B.; Diao, J.; Jiang, Y. Enhanced adsorption of cadmium from aqueous solution by amino modification biochar and its adsorption mechanism insight. *J. Environ. Chem. Eng.* **2023**, *11*, No. 109747.
(39) Ho, Y. S.; Ng, J. C. Y.; McKay, G. Kinetics of pollutant sorption by biosorbents: review. *Sep. Purif. Methods* **2000**, *29*, 189−232.
(40) Gao, F.; Li, J.; Sun, C.; Zhang, L.; Jiang, F.; Cao, W.; Zheng, L. Study on the capability and characteristics of heavy metals enriched on microplastics in marine environment. *Mar. Pollut. Bull.* **2019**, *144*, 61−67.
(41) Wang, F.; Yang, W.; Cheng, P.; Zhang, S.; Zhang, S.; Jiao, W.; Sun, Y. Adsorption characteristics of cadmium onto microplastics from aqueous solutions. *Chemosphere* **2019**, *235*, 1073−1080.
(42) Fierro, V.; Torné-Fernández, V.; Montané, D.; Celzard, A. Adsorption of phenol onto activated carbons having different textural and surface properties. *Microporous Mesoporous Mater.* **2008**, *111*, 276−284.
(43) Wang, J.; Guo, X. Adsorption isotherm models: Classification, physical meaning, application and solving method. *Chemosphere* **2020**, *258*, No. 127279.
(44) Han, B. *Microplastics Influence the Adsorption and Desorption Characteristics of Heavy Metals in Soil*; Qingdao University of Science & Technology, 2020.
(45) Wang, X. *Effect of Microplastics on the Adsorption and Desorption of Zinc in Soil*; Qingdao University of Science & Technology, 2021.
(46) Wu, Q.; Chen, J.; Clark, M.; Yu, Y. Adsorption of copper to different biogenic oyster shell structures. *Appl. Surf. Sci.* **2014**, *311*, 264−272.
(47) Lin, Z.; Hu, Y.; Yuan, Y.; Hu, B.; Wang, B. Comparative analysis of kinetics and mechanisms for Pb (II) sorption onto three kinds of microplastics. *Ecotoxicol. Environ. Saf.* **2021**, *208*, No. 111451.
(48) Fu, Q.; Hu, B.; Zhou, X.; Hu, Q.; Sheng, J. Impact of key geochemical parameters on the attenuation of Pb (II) from water using a novel magnetic nanocomposite: fulvic acid-coated magnetite nanoparticles. *Desalin. Water Treat.* **2016**, *57*, 26063−26072.
(49) Shen, M.; Song, B.; Zeng, G.; Zhang, Y.; Teng, F.; Zhou, C. Surfactant changes lead adsorption behaviors and mechanisms on microplastics. *Chem. Eng. J.* **2021**, *405*, No. 126989.
(50) Qin, F.; Wen, B.; Shan, X.; Xie, Y.; Liu, T.; Zhang, S.; Khan, S. U. Mechanisms of competitive adsorption of Pb, Cu, and Cd on peat. *Environ. Pollut.* **2006**, *144*, 669−680.
(51) Jalali, M.; Moradi, F. Competitive sorption of Cd, Cu, Mn, Ni, Pb and Zn in polluted and unpolluted calcareous soils. *Environ. Monit. Assess.* **2013**, *185*, 8831−8846.
(52) Yang, Z.; Shi, H.; Wang, H.; Zuo, N.; Mengting, Z.; Wang, L. Competitive adsorption behavior and mechanism toward Pb and Cd at different tier soil profiles. *Chin. J. Soil Sci.* **2017**, *48*, 730−735.
(53) Tang, S.; Lin, L.; Wang, X.; Feng, A.; Yu, A. Pb(II) uptake onto nylon microplastics: Interaction mechanism and adsorption performance. *J. Hazard. Mater.* **2020**, *386*, No. 121960.
(54) Guo, W.; Dai, J.; Wang, R. Progress in the effect of dissolved organic matter on adsorption of heavy metals by soil. *Chin. J. Soil Sci.* **2012**, *43*, 761−768.
(55) Jiao, W.; Jiang, X.; Huang, J. Heavy Metal Contaminated Soil Treatment and Ecological Remediation Forum 2012 (China-Beijing). 2012, pp 89−90.
(56) Jordan, R. N.; Yonge, D. R.; Hathhorn, W. E. Enhanced mobility of Pb in the presence of dissolved natural organic matter. *J. Contam. Hydrol.* **1997**, *29*, 59−80.
(57) Chen, T.; Huang, Z.; Chen, H. Effect of DOMs extracted from five solid organic wastes on cadmium adsorption in soils. *Acta Sci. Circumstantiae* **2002**, 150−155.
(58) Kong, D. Adsorption characteristic of Cu on loess soil affected by humic acid. *Guangdong Chem. Ind.* **2014**, *41*, 41−42.
(59) Lin, Y.; Gong, X.; Xiong, J.; Wu, L.; Zeng, H. Effects of DOM on wetland soil adsorption of heavy metals Pb^{2+} and Cd^{2+}. *J. Nanchang Univ.* **2021**, *45*, 71−78.
(60) Chen, W.; Ouyang, Z. Y.; Qian, C.; Yu, H. Q. Induced structural changes of humic acid by exposure of polystyrene microplastics: A spectroscopic insight. *Environ. Pollut.* **2018**, *233*, 1−7.
(61) Abdurahman, A.; Cui, K.; Wu, J.; Li, S.; Gao, R.; Dai, J.; Liang, W.; Zeng, F. Adsorption of dissolved organic matter (DOM) on polystyrene microplastics in aquatic environments: Kinetic, isotherm and site energy distribution analysis. *Ecotoxicol. Environ. Saf.* **2020**, *198*, No. 110658.
(62) Guan, Y.; Gong, J.; Song, B.; Li, J.; Fang, S.; Tang, S.; Cao, W.; Li, Y.; Chen, Z.; Ye, J.; Cai, Z. The effect of UV exposure on conventional and degradable microplastics adsorption for Pb (II) in sediment. *Chemosphere* **2022**, *286*, No. 131777.
(63) Guo, X.; Hu, G.; Fan, X.; Jia, H. Sorption properties of cadmium on microplastics: The common practice experiment and A two-dimensional correlation spectroscopic study. *Ecotoxicol. Environ. Saf.* **2020**, *190*, No. 110118.
(64) Browne, M. M.; Lubarsky, G. V.; Davidson, M. R.; Bradley, R. H. Protein adsorption onto polystyrene surfaces studied by XPS and AFM. *Surf. Sci.* **2004**, *553*, 155−167.

https://doi.org/10.1021/acsomega.4c03809
ACS Omega 2024, 9, 32021−32032

(65) Guo, X.; Pang, J.; Chen, S.; Jia, H. Sorption properties of tylosin on four different microplastics. *Chemosphere* **2018**, *209*, 240−245.

https://doi.org/10.1021/acsomega.4c03809
ACS Omega 2024, 9, 32021−32032